Twisted-Light–Ion Interaction: The Role of Longitudinal Fields

G. F. Quinteiro,[1,*] Ferdinand Schmidt-Kaler,[2] and Christian T. Schmiegelow[1]
[1]Departamento de Física and IFIBA, FCEN, Universidad de Buenos Aires, Ciudad Universitaria, Pabellón I, 1428 Ciudad de Buenos Aires, Argentina
[2]QUANTUM, Institut für Physik, Universität Mainz, Staudingerweg 7, 55128 Mainz, Germany
(Received 15 July 2017; published 20 December 2017)

The propagation of light beams is well described using the paraxial approximation, where field components along the propagation direction are usually neglected. For strongly inhomogeneous or shaped light fields, however, this approximation may fail, leading to intriguing variations of the light-matter interaction. This is the case of twisted light having opposite orbital and spin angular momenta. We compare experimental data for the excitation of a quadrupole transition in a single trapped $^{40}Ca^{+}$ ion from Schmiegelow *et al.* [Nat. Commun. **7**, 12998 (2016)] with a complete model where longitudinal components of the electric field are taken into account. Our model matches the experimental data and excludes by 11 standard deviations the approximation of a complete transverse field. This demonstrates the relevance of all field components for the interaction of twisted light with matter.

DOI: 10.1103/PhysRevLett.119.253203

The vector character of the electromagnetic field is responsible for a variety of basic physical processes, such as those occurring in near-field optics and the propagation of focused beams close to the diffraction limit [1,2]. Moreover, electromagnetic fields with components in all possible directions play a special role in applied science. For example, the sub-diffraction-limited focusing of radially polarized beams producing strong longitudinal fields [3] can be used to improve material processing [4,5]. Also, longitudinal fields have seen application in Raman spectroscopy [6], and optical tweezers [7], and have been used to observe circular dichroism in nonchiral nanostructures [8].

Light carrying orbital angular momentum, known also as twisted light or optical vortices, has introduced us to a new realm of structured light [9–14]. An unusual property of twisted light has to do with the relative orientation of the photon's angular momenta. When the orbital and spin angular momenta are antiparallel to each other, longitudinal field components become important. As a result, the light-matter interaction is different for parallel or antiparallel momenta beams. This has been suggested in several theoretical articles dealing with tightly focused twisted light [15,16] and twisted light-related beams [17–21]. Longitudinal fields in structured beams promise new applications, such as the control of the spin state of electrons or impurities in quantum dots [15,22], and the excitation of intersubband [23] transitions in quantum wells [24].

For propagating fields that are not tightly focused, the complexity of the full vector model can be reduced while still retaining an excellent description of the physics under consideration. In the paraxial approximation [25] one assumes that the transverse profile changes slowly along the z direction. To lowest order in the ratio of wavelength to beam waist the electric and magnetic fields have no longitudinal component [26,27]. Although very common, such a strong assumption is not always correct. Theory shows that Laguerre-Gaussian (LG) beams, the most extensively used paraxial twisted light, have a non-negligible longitudinal component when spin and orbital angular momenta are opposite to each other [26,28]. An intuitive ray-tracing argument helps understand why longitudinal fields play an important role. A transverse cut of the electric field shows a clear difference between the situation where the orbital angular momentum ℓ is parallel or antiparallel to the spin degree of freedom or circular polarization σ of a vortex light field, see Figs. 1(a) and 1(b), respectively. Following rays through a lens the field will interfere destructively or constructively depending on whether ℓ and σ point in the same or opposite directions, producing a corresponding negligible or appreciable longitudinal field component.

In this Letter we show that the correct description of the light-matter interaction between a single ion and a paraxial LG beam requires the inclusion of the longitudinal electric-field component, when the beam is in the antiparallel momenta configuration. Thus, longitudinal field components do matter even in the paraxial approximation, and may lead to unexpected applications, for example, to chiral quantum optics [29–31].

Before engaging in the light-matter model and a comparison with experiments, we briefly discuss Laguerre-Gaussian modes. These modes are solutions of the paraxial wave equation in cylindrical coordinates, and are perhaps the most studied of all optical-vortex beams, for they can be easily produced from conventional laser beams using computer generated holograms, cylindrical lenses, Q plates, etc. [32]. The starting point for the derivation of the electromagnetic field is a transverse Lorentz-gauge vector potential $\mathbf{A}(\mathbf{r},t) = A_0 \boldsymbol{\epsilon} u(\mathbf{r}) \exp(-i\omega t + ikz) + \text{c.c.}$ with polarization $\boldsymbol{\epsilon} = \epsilon_x \hat{x} + \epsilon_y \hat{y}$, wave number in the longitudinal direction k, amplitude A_0, and mode $u(\mathbf{r})$ constructed from a

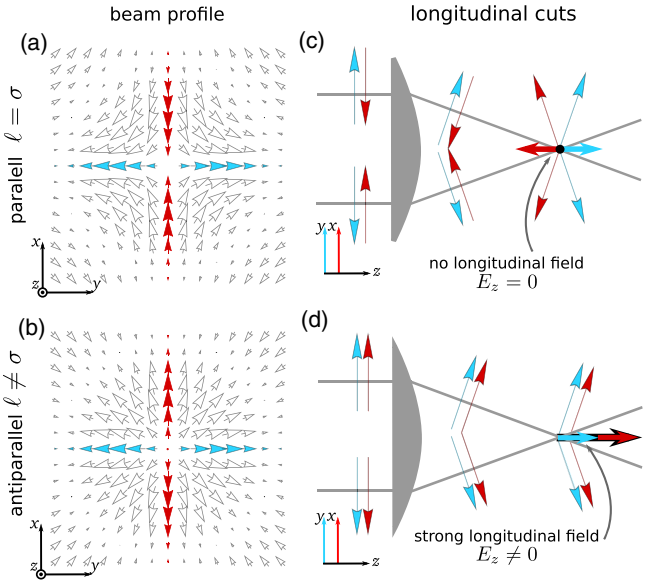

FIG. 1. Illustration of how different beams may or may not have a longitudinal field component. (a),(b) Transverse cut of Laguerre-Gaussian beams with orbital angular momentum $\ell = 1$ and different spin or circular polarization $\sigma = \pm 1$. In the top rows (a) and (c) the spin and orbital angular momentum are parallel; in the bottom rows (b) and (d) they are antiparallel. The arrows indicate the projection of the field direction on this plane. (c),(d) The beam as it propagates after a lens. At the focus position the resulting component at the center of the beam is drawn in black. When the spin and orbital angular momentum are parallel there is no longitudinal component. Conversely, when they are antiparallel, there is a strong longitudinal component. The interference giving rise to a longitudinal component can be understood as well from a modal decomposition of the beam.

combination of a generalized Laguerre polynomial, a Gaussian function, a polynomial, and a phase factor [32–34]. In problems involving the interaction with small objects that are centered with respect to the beam axis the full lateral spatial extent of the beam is irrelevant, and one can simplify the beam's profile to $u(\mathbf{r}) \propto r^{|\ell|} e^{i\ell\varphi}$ in cylindrical coordinates $\{r, \varphi, z\}$ with ℓ the orbital angular momentum index [35]. This simplification is valid for a quasipointlike atomic wave packet [36].

Using the Lorenz condition, a scalar potential can be deduced. From vector and scalar potentials, the electric and magnetic fields are calculated, see the Supplemental Material [37]. The positive-frequency part of the electric field of a circularly polarized LG beam close to the phase singularity at $r = 0$ is

$$\mathbf{E}_{\perp}^{(+)}(\mathbf{r}) = (\hat{x} + i\sigma\hat{y}) \frac{E_0}{\sqrt{\pi|\ell|!}w_0} \left(\frac{\sqrt{2}}{w_0} r\right)^{|\ell|} e^{i\ell\varphi} e^{ikz}, \tag{1a}$$

$$E_z^{(+)}(\mathbf{r}) = -i(\ell\sigma - |\ell|)(1 - \delta_{\ell,0}) \frac{E_0}{\sqrt{\pi|\ell|!}w_0} \frac{\sqrt{2}}{w_0 k} \times \left(\frac{\sqrt{2}}{w_0} r\right)^{|\ell|-1} e^{i(\ell+\sigma)\varphi} e^{ikz}, \tag{1b}$$

where we have separated it into transverse $\mathbf{E}_{\perp}^{(+)}(\mathbf{r})$ and longitudinal $E_z^{(+)}(\mathbf{r})$ components. Here, $\mathbf{E}(\mathbf{r}, t) = \mathbf{E}^{(+)}(\mathbf{r}) e^{-i\omega t} + \text{c.c.}$, $\sigma = \pm 1$ is the spin index or handedness of circular polarization, and E_0 is the amplitude. One can directly see that the longitudinal component is only present when spin and orbital angular momenta are counterrotating, i.e., for $(\ell\sigma - |\ell|) = -2|\ell|$. In this situation it is in fact crucial to take into account the longitudinal field to accurately describe quantitatively the atom-photon interaction. Also clear is that $E_z^{(+)}(\mathbf{r})$ is of higher order in the paraxial parameter $1/(w_0 k)$.

Intriguing features of light fields can be sensed by matter, especially by atoms [38–41]. However, to unveil all possible effects, an accurate theory of light-matter interaction that accounts for the full vector properties of the beam is needed. We will consider the interaction of twisted light with a single atom or ion. The particle is assumed to be cooled below its Lamb-Dicke limit, so neglecting linear momentum transfer to the atom's center of mass is well justified.

In the experiment we analyze [36], a LG beam with a wavelength near $\lambda = 729$ nm and $|\ell| = 0, 1$ was focused to $w_0 = 2.7$ μm onto a single ion. This focus size is well above the optical diffraction limit. The ion was laser cooled to a wave packet position uncertainty of $\Delta r = 60$ nm, and positioned at the center of the vortex field, and the quadrupole $S_{1/2}$ to $D_{5/2}$ transition was excited.

In this situation, light-matter interaction is dominated by the electric field. Thus, in the Poincaré gauge, the interaction Hamiltonian $H_I = qU(\mathbf{r}, t)$ results from the scalar potential $U(\mathbf{r}, t) = -\int_0^1 \mathbf{r} \cdot \mathbf{E}(u\mathbf{r}, t) du$ [42]. The oscillating time dependence in $H_I = H_I^{(+)} e^{-i\omega t} + \text{c.c.}$ may be omitted, as the positive-frequency part $H_I^{(+)}$ is sufficient to calculate transition matrix elements in the rotating wave approximation [43]. Using the explicit expressions for the electric field, Eqs. (1a) and (1b), transforming to spherical coordinates $\{\rho, \varphi, \theta\}$, and separating the interaction Hamiltonian into in-plane and z sections results in the following Hamiltonians. For $\ell = 0$

$$H_{I\perp}^{(+)} = -\alpha\rho \sin(\theta) e^{i\sigma\varphi} \int_0^1 u e^{iku\rho\cos(\theta)} du, \tag{2a}$$

$$H_{Iz}^{(+)} = 0, \tag{2b}$$

where $\alpha = \sqrt{2/\pi} q E_0 / w_0^2$ with $q = -|q_e|$ the electric charge. For $\ell = \pm 1$

$$H_{I\perp}^{(+)} = -\alpha\rho^2 \sin^2(\theta) e^{i(|\ell|/\ell+\sigma)\varphi} \int_0^1 u e^{iku\rho\cos(\theta)} du, \tag{3a}$$

$$H_{Iz}^{(+)} = -i\delta_{\ell,-\sigma} \alpha\rho\cos(\theta) \frac{2}{k} \int_0^1 e^{iku\rho\cos(\theta)} du. \tag{3b}$$

Under the experimental conditions considered, and due to the small size of the atom with respect to the wavelength of the exciting laser, a Taylor approximation of $\exp[iku\rho\cos(\theta)]$ is justified. However, the expansion has to be treated differently for the in-plane and z sections of the interaction. We will be concentrating on quadrupole transitions where the initial and final state have the same parity. This causes the transition matrix elements to vanish at first order in the coordinates. The matrix elements that govern these transitions are those with quadratic dependence on the coordinates.

When $\ell = 0$ the transitions allowed by angular momentum selection rules are those with a change in projection of angular momentum in the z direction: $\Delta m = \pm 1$. In Fig. 2(a) these are labeled $\{b, d\}$ and $\{g, i\}$. These transitions are governed by Eq. (2a). The zero-order term in the expansion of the exponential yields a Hamiltonian linear in the coordinates, and vanishes for the quadrupole transition. The transition is thus mediated by the following term in the expansion: $H_{I\perp}^{(+)} \simeq -i(\alpha k\rho^2/3)\sin(\theta)\cos(\theta)e^{i\sigma\varphi}$.

In the case $\ell = \pm 1$, in-plane and/or longitudinal interactions may induce the transitions with no change or a change of two units of angular momentum of the ion ($\Delta m = 0, \pm 2$) depending on the signs of the polarization (σ) and the sense of rotation of the LG beam (the sign of ℓ). These transitions are labeled $\{a, c, e\}$ and $\{f, h, j\}$ in Fig. 2(a). Following the same reasoning as before, we must consider the first-order term $\exp[iku\rho\cos(\theta)] \simeq iku\rho\cos(\theta)$ for transitions induced by H_{Iz}, but it suffices to consider the zero-order term $\exp[iku\rho\cos(\theta)] \simeq 1$ for $H_{I\perp}$.

It is worth noting that even though different approximations to $\exp[iku\rho\cos(\theta)]$ were used, both interaction terms $H_{I\perp}^{(+)}$ and $H_{Iz}^{(+)}$ are of the same magnitude, a fact that will become evident when the numerical evaluations are performed. Moreover, the ratio of these two components does not depend on the focus size.

We contrast our theory with the measured interaction strengths of different quadrupole transitions of a single trapped calcium ion induced by LG beams, as reported in the above-mentioned experiment of Ref. [36]. In particular we concentrate on the experiments where the trapped ion is illuminated by on-center LG beams with different polarizations. (We note that analyses of the effects of off-centered beams have been released during the review of this Letter [44,45]). The frequency of the LG beam is tuned to the different magnetic sublevels of the $4S_{1/2}$-$3D_{5/2}$ transition, which are Zeeman split by a static magnetic field in the z direction [see Fig. 2(a)]. Transitions with a different change in atom angular momentum $\Delta m = -2$, -1, 0, 1, 2 were excited with all combinations of spin and orbital angular momentum of the beam $m_p = \sigma + \ell$. Here, we restrict ourselves to the cases where the total angular momentum of the photon matches the change of angular

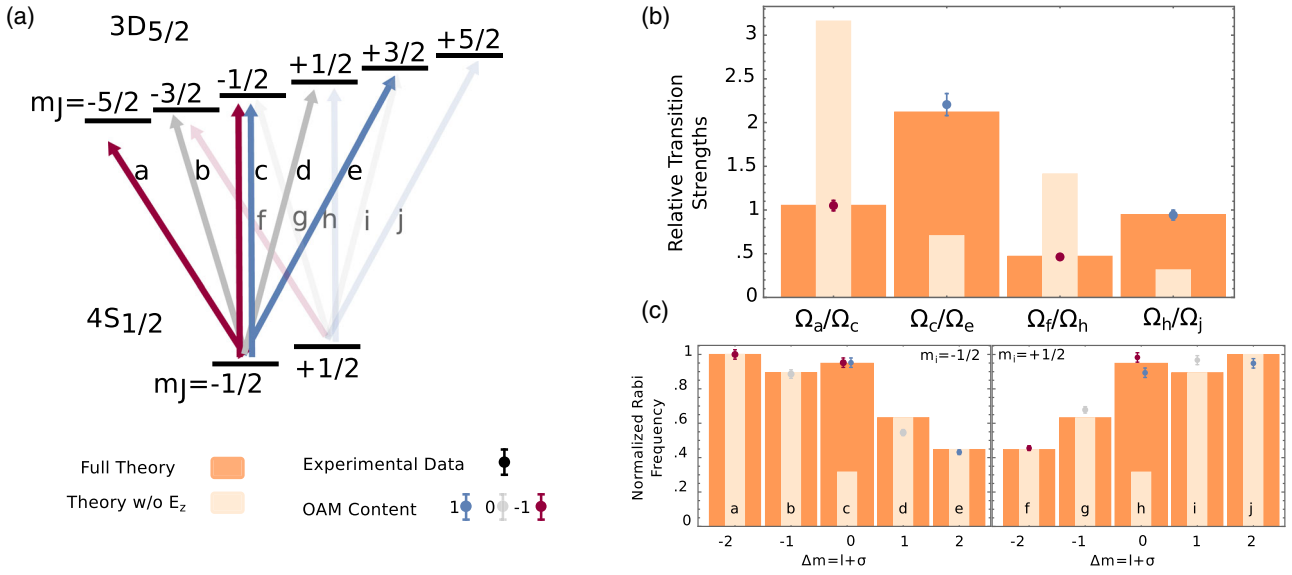

FIG. 2. (a) Energy levels for the Zeeman split $^{40}Ca^{+}$ quadrupole $S_{1/2}$-$D_{5/2}$ transition. The transitions are labeled from a to j and shown in different colors indicating the photon orbital angular momentum content. Note that there are two different configurations to drive the $\Delta m = 0$ transitions, either with $\ell = +1$ or -1. (b) Relative transition strengths expressed as ratios of Rabi frequencies Ω for different transitions. Data for the $\ell = 1$ transitions (light blue) and for the $\ell = -1$ transitions (dark purple) are plotted together with theory predictions. Dark orange bars show the prediction with the model presented in this Letter where longitudinal fields are taken into account. Light orange bars show the prediction where the longitudinal field is neglected. (c) Normalization is done to a chosen transition Ω_a and to account for the difference in interaction strength between transitions driven with Gaussian or vortex beams with $\Omega_{\text{norm}} = \Omega_a(\delta_{|\ell|,1} + \delta_{\ell,0}kw_0)$. All measured transition strengths and predictions are labeled as in (a).

momentum of the atom $\Delta m = m_p$. The experiments determined the strength of each transition by measuring the frequency Ω_γ of its Rabi oscillations by state-dependent fluorescence [46].

We calculate matrix elements $M_\gamma = \langle 3D_{5/2}, m_{j'}|H_I(\ell,\sigma)|4S_{1/2}, m_j\rangle$ for all transitions following Ref. [47] and as detailed in the Supplementary Material [37]. The Rabi frequencies are proportional to the matrix elements M_γ of the given transition, $\Omega_\gamma \propto M_\gamma$, with the same proportionality factor for all of them. The uncertainty in the determination of an absolute interaction strength can be eliminated by calculating quotients of matrix elements. In the language of the Wigner-Eckart theorem, as all matrix elements share the same initial and final radial and total angular momentum quantum numbers, the reduced matrix element is the same for all M_γ. Thus, the ratio of matrix elements depends only on the angular part of the matrix elements.

Following this idea, we compare quotients of matrix elements to quotients of experimental Rabi frequencies. Figure 2(b) shows the ratios of transitions induced by beams with opposite polarization and orbital angular momentum. We analyze both possible initial states ($m_j = \pm 1/2$) and both possible $\ell = \pm 1$. Together with the data, we plot the predictions with and without the longitudinal field. We see that the results match the theory with the full vector field. The incomplete theory with no E_z is off in all cases by more than 11 standard deviations.

A different comparison of all transitions strengths is shown in Fig. 2(c). Here, the relative interaction strengths are calculated with respect to transition a (any other could be chosen without loss of generality). One clearly sees that the prediction that does not include the longitudinal field dramatically fails for the case of counterrotating spin and orbital angular momentum, when $\Delta m = 0$. We note that, due to systematic errors introduced in changing the beam type, there is a small difference between theory and experiment in some cases. This happens because changing the beam type requires realignment and correction of the beam focus. This is not present when the only change is in the polarization as the quotients show in Fig. 2(b).

The interaction of matter with strongly inhomogeneous fields shows complex features and exposes new physics [48–55]. Our results on the interaction of Laguerre-Gaussian modes with single ions demonstrate that an extremely good quantitative match between predictions and measurements is achieved only if an improved version of the paraxial approximation is used, where the longitudinal field is taken into account. In contrast, a theory that lacks the longitudinal component misses the experimental values for up to 11 standard deviations.

Longitudinal fields are important in quantum optics setups, such as with trapped ions, but also well beyond as, for instance, with neutral atoms, molecules, and quantum dots. Our finding of the significance of longitudinal fields may pave new ways to manipulate matter for spintronics, nanophotonics, and quantum information. But besides possible new uses, countless applications thought to be implemented by more technically demanding tools of near-field optics or tight focusing may become addressable by simple beams of twisted light. One important example is the chiral light-matter interaction from the longitudinal component of light propagating in subwavelength waveguides to produce directional coupling in nanophotonic chips [29]. In the future, we plan to explore chiral coupling effects from free-propagating LG light beams, specifically for the different platforms of trapped ions or colloidal quantum dots.

G. F. Q. thanks Agencia Nacional de Promoción Científica y Tecnológica (ANPCyT) for financial support through PICT 2013-0592, F. S. K. thanks the DFG for financial support in the DIP program (FO 703/2-1), and C. T. S. acknowledges the support from the Alexander von Humboldt Foundation and the Fundación Bunge y Born.

*gquinteiro@df.uba.ar

[1] L. Novotny and B. Hecht, *Principles of Nano-Optics* (Cambridge University Press, Cambridge, England, 2012).
[2] Q. Zhan, *Vectorial Optical Fields: Fundamentals and Applications* (World Scientific, Singapore, 2013).
[3] R. Dorn, S. Quabis, and G. Leuchs, Phys. Rev. Lett. **91**, 233901 (2003).
[4] H. Wang, L. Shi, B. Lukyanchuk, C. Sheppard, and C. T. Chong, Nat. Photonics **2**, 501 (2008).
[5] M. Meier, V. Romano, and T. Feurer, Appl. Phys. A **86**, 329 (2007).
[6] Y. Saito, M. Kobayashi, D. Hiraga, K. Fujita, S. Kawano, N. Smith, Y. Inouye, and S. Kawata, J. Raman Spectrosc. **39**, 1643 (2008).
[7] Q. Zhan, Opt. Express **12**, 3377 (2004).
[8] X. Zambrana-Puyalto, X. Vidal, and G. Molina-Terriza, Nat. Commun. **5**, 4922 (2014).
[9] L. Allen, M. W. Beijersbergen, R. J. C. Spreeuw, and J. P. Woerdman, Phys. Rev. A **45**, 8185 (1992).
[10] M. Padgett, J. Courtial, and L. Allen, Phys. Today **57**, No. 5, 35 (2004).
[11] D. L. Andrews and M. Babiker, *The Angular Momentum of Light* (Cambridge University Press, Cambridge, England, 2012).
[12] M. J. Padgett, Opt. Express **25**, 11265 (2017).
[13] S. Franke-Arnold and N. Radwell, Opt. Photonics News **28**, 28 (2017).
[14] H. Rubinsztein-Dunlop *et al.*, J. Opt. **19**, 013001 (2017).
[15] G. F. Quinteiro and T. Kuhn, Phys. Rev. B **90**, 115401 (2014).
[16] G. F. Quinteiro, D. E. Reiter, and T. Kuhn, Phys. Rev. A **91**, 033808 (2015).
[17] N. Bokor, Y. Iketaki, T. Watanabe, and M. Fujii, Opt. Express **13**, 10440 (2005).
[18] Y. Iketaki, T. Watanabe, N. Bokor, and M. Fujii, Opt. Lett. **32**, 2357 (2007).

[19] P. B. Monteiro, P. A. M. Neto, and H. M. Nussenzveig, Phys. Rev. A **79**, 033830 (2009).
[20] V. V. Klimov, D. Bloch, M. Ducloy, and J. R. R. Leite, Phys. Rev. A **85**, 053834 (2012).
[21] J. R. Zurita-Sánchez and L. Novotny, J. Opt. Soc. Am. B **19**, 2722 (2002).
[22] E. Pazy, E. Biolatti, T. Calarco, I. D'amico, P. Zanardi, F. Rossi, and P. Zoller, Europhys. Lett. **62**, 175 (2003).
[23] B. Sbierski, G. Quinteiro, and P. Tamborenea, J. Phys. Condens. Matter **25**, 385301 (2013).
[24] L. West and S. Eglash, Appl. Phys. Lett. **46**, 1156 (1985).
[25] A. E. Siegman, *Lasers* (University Science Books, Mill Valley, CA, 1986), p. 276.
[26] M. Lax, W. H. Louisell, and W. B. McKnight, Phys. Rev. A **11**, 1365 (1975).
[27] C. G. Chen, P. T. Konkola, J. Ferrera, R. K. Heilmann, and M. L. Schattenburg, J. Opt. Soc. Am. A **19**, 404 (2002).
[28] S. M. Barnett and L. Allen, Opt. Commun. **110**, 670 (1994).
[29] P. Lodahl, S. Mahmoodian, S. Stobbe, A. Rauschenbeutel, P. Schneeweiss, J. Volz, H. Pichler, and P. Zoller, Nature (London) **541**, 473 (2017).
[30] B. Vermersch, P.-O. Guimond, H. Pichler, and P. Zoller, Phys. Rev. Lett. **118**, 133601 (2017).
[31] M. Nieto-Vesperinas, Phil. Trans. R. Soc. A **375**, 20160314 (2017).
[32] D. L. Andrews, *Structured Light and Its Applications: An Introduction to Phase-Structured Beams and Nanoscale Optical Forces* (Academic Press, New York, 2008).
[33] R. Loudon, Phys. Rev. A **68**, 013806 (2003).
[34] L. Allen, M. J. Padgett, and M. Babiker in *Progress in Optics* 39, edited by E. Wolf (Elsevier, New York, 1999), p. 294.
[35] G. F. Quinteiro, A. O. Lucero, and P. I. Tamborenea, J. Phys. Condens. Matter **22**, 505802 (2010).
[36] C. T. Schmiegelow, J. Schulz, H. Kaufmann, T. Ruster, U. G. Poschinger, and F. Schmidt-Kaler, Nat. Commun. **7**, 12998 (2016).
[37] See Supplemental Material at http://link.aps.org/supplemental/10.1103/PhysRevLett.119.253203 for detailed derivations of the electric field and the evaluation of matrix elements using the Wigner-Eckard theorem.
[38] H. M. Scholz-Marggraf, S. Fritzsche, V. G. Serbo, A. Afanasev, and A. Surzhykov, Phys. Rev. A **90**, 013425 (2014).
[39] P. K. Mondal, B. Deb, and S. Majumder, Phys. Rev. A **89**, 063418 (2014).
[40] A. Afanasev, C. E. Carlson, and M. Solyanik, J. Opt. **19**, 105401 (2017).
[41] A. Surzhykov, D. Seipt, V. G. Serbo, and S. Fritzsche, Phys. Rev. A **91**, 013403 (2015).
[42] G. F. Quinteiro, D. E. Reiter, and T. Kuhn, Phys. Rev. A **95**, 012106 (2017).
[43] M. O. Scully and M. S. Zubairy, *Quantum Optics* (Cambridge University Press, Cambridge, England, 1997).
[44] A. A. Peshkov, D. Seipt, A. Surzhykov, and S. Fritzsche, Phys. Rev. A **96**, 023407 (2017).
[45] A. Afanasev, C. E. Carlson, C. T. Schmiegelow, J. Schulz, F. Schmidt-Kaler, and M. Solyanik, arXiv:1709.05571.
[46] T. Sauter, W. Neuhauser, R. Blatt, and P. E. Toschek, Phys. Rev. Lett. **57**, 1696 (1986).
[47] C. Schmiegelow and F. Schmidt-Kaler, Eur. Phys. J. direct D **66**, 1 (2012).
[48] K. Koksal and F. Koc, Comput. Theor. Chem. **1099**, 203 (2017).
[49] K. Shigematsu, K. Yamane, R. Morita, and Y. Toda, Phys. Rev. B **93**, 045205 (2016).
[50] B. Thidé, F. Tamburini, H. Then, C. G. Someda, and R. A. Ravanelli, arXiv:1410.4268.
[51] M. A. Noyan and J. M. Kikkawa, Appl. Phys. Lett. **107**, 032406 (2015).
[52] J. Watzel and J. Berakdar, Sci. Rep. **6**, 21475 (2016).
[53] C. Hernandez-Garcia, J. Vieira, J. T. Mendonca, L. Rego, J. S. Roman, L. Plaja, P. R. Ribic, D. Gauthier, and A. Picon, Photonics **4**, 28 (2017).
[54] X. Zang and M. T. Lusk, Phys. Rev. A **96**, 013819 (2017).
[55] M. Inglot and V. Dugaev, Acta Phys. Pol. A **132**, 193 (2017).